Geophysical Journal International

Geophys. J. Int. (2023) **234,** 2437–2445
Advance Access publication 2023 April 28
GJI Seismology

https://doi.org/10.1093/gji/ggad171

Tsunami initial profile and maximum runup through earthquake source parameters

Naeimeh Sharghivand [1] and Utku Kânoğlu [2,*]

[1] *Department of Engineering Sciences, Middle East Technical University, Ankara, Turkey. E-mail: na.sharghivand@gmail.com*
[2] *Department of Aerospace Engineering, Dokuz Eylül University, İzmir, Turkey . E-mail: utku.kanoglu@deu.edu.tr*

Accepted 2023 April 17. Received 2023 April 17; in original form 2022 August 2

SUMMARY

The 1992 September 1 Nicaragua tsunami manifested itself with an initial shoreline recession, resulting in a fundamental change in approach to define the initial waveform of tsunamis from a solitary wave to an *N*-wave. Here, we first fit *N*-wave profile to seafloor deformation for a large set of earthquake scenarios, assuming that the seafloor deformation resulting from an earthquake instantaneously transfers to the sea surface. Then, relating the *N*-wave parameters to the earthquake source parameters, we express the initial tsunami profile in terms of the earthquake source parameters. Further, we calculate the maximum tsunami runup through earthquake source parameters and test our results against field runup measurements for several events, observing good agreement.

Key words: Tsunamis; Earthquake source observations; Tsunami warning; *N*-wave; Rapid tsunami runup forecast.

1 INTRODUCTION

Tsunamis can be high-impact, long-duration catastrophes, often with multiple devastating waves penetrating target coastlines (Kânoğlu *et al.* 2015). Once a tsunami is generated, waves can travel long distances leading to coastal inundation not only in the near-field, but also in far-field, for example, the energy propagation maps of the 2004 December 26 Sumatra (Titov *et al.* 2005) and the 2011 March 11 Japan (Tang *et al.* 2012) tsunamis. Field observations from past tsunami disasters have always proved the importance of warning time, especially in nearshore tsunami forecasting. The arrival time of the tsunami at the nearest coastline to the earthquake epicentre is exceedingly short. Hence, providing a reliable warning within minutes of the event is crucial to saving lives.

At present, most of the near- and far-field tsunami forecast models employ tsunami numerical modelling (Imamura & Imteaz 1995; Liu *et al.* 1998; Tinti & Tonini 2013; Miranda *et al.* 2014; Titov *et al.* 2016). In addition, probabilistic tsunami hazard assessment (PTHA) has been used to estimate tsunami hazard potential on a nationwide or global scale (González *et al.* 2009; Grezio *et al.* 2017; Behrens *et al.* 2022).

Numerical models require high-resolution bathymetric and topographic data as input. In addition to the high-resolution geospatial data, if a high-performance computing cluster is not accessible for real-time computing, numerical modelling might not be effective in forecasting the impact of nearshore tsunamis. However, numerical models and PTHA can be beneficial in providing tsunami hazard maps (Borrero *et al.* 2003; Walsh *et al.* 2004; Schlurmann *et al.* 2010; Davies & Griffin 2019) and estimating potential tsunami hazard for at-risk communities (Harbitz *et al.* 2016; Lynett *et al.* 2017; Sepúlveda *et al.* 2019; Yalçıner *et al.* 2019; Aydın *et al.* 2020) in pre-hazard action planning.

Alongside numerical models and PTHA, an amplification factor method, i.e. relating the offshore wave height to the maximum inundation height, is used to provide faster estimates of the tsunami height (Løvholt *et al.* 2012; Baba *et al.* 2014; Løvholt *et al.* 2016; Glimsdal *et al.* 2019).

Reviewing studies relating earthquake source parameters to tsunami maximum runup, Okal & Synolakis (2004) used a data set of 72 models of nearshore seismic dislocations and landslide sources, and performed numerical simulations. They varied fault parameters one by one and presented their effects on tsunami runup height. However, their main goal was to identify source discriminants to distinguish landslide and earthquake generated events. Geist (1998) investigated the relationship between earthquake source parameters and *N*-wave characteristics but did not present explicit relationships. Sepúlveda & Liu (2016) presented two relationships between the tsunami runup height and seismic parameters, for boundary-value problem through Madsen & Schäffer (2010) formulation and for initial-value problem solution through Kânoğlu (2004). They applied their approach to the 2004 Sumatra and 2010 Chile tsunamis.

*This work was mostly conducted when Author was affiliated with the Middle East Technical University, Ankara, Turkey

In a recent study, Wronna *et al.* (2021) obtained a new parameter, calling tsunami runup predictor (TRP), and proposed relationships between TRP and maximum runup for leading elevation *N*-wave (LEN) and leading depression *N*-wave (LDN). They developed the initial tsunami waveforms for different scenarios by adjusting the fault plane parameters and also by varying the source distance to the shore and the beach slope. Then, they used the numerical (Miranda & Luis 2019) and the analytical (Aydın & Kânoğlu 2017) methods to calculate tsunami runup on constant beach slopes. Wronna *et al.* (2021) then compared TRP estimates to the field measurements of several past tsunami events and obtained good estimates.

Synolakis & Bernard (2006) named the decade from 1990 to 2000 as the 'tsunami decade' considering the unusual number of tsunami occurrences in this period. During the field surveys of these events conducted by International Tsunami Survey Teams, nearly all eyewitnesses reported shoreline recession before waves advanced up the coasts. This resulted in a fundamental change from a solitary wave to an *N*-wave as a more realistic initial waveform of tsunamis. Consequently, Tadepalli & Synolakis (1994) suggested classes of waves, called *N*-waves, to describe the evolution and runup of nearshore tsunamis. They defined two particular classes of *N*-waves: LDNs and LENs, and showed that LDNs run up higher than their mirror image, LENs. They suggested LDNs as a more appropriate initial waveform for nearshore tsunamis. After Tadepalli & Synolakis's (1994) introduction of *N*-waves as a realistic initial waveform of incoming tsunamis, it took several more events for the community to accept it (Madsen & Schäffer 2010). Nonetheless, Tadepalli & Synolakis (1996) incorporated a steepness parameter and proved the *N*-waves as a geophysically realistic model for long-wave propagation particularly tsunamis.

We seek to explore more expeditious forecasting, and we thus present a new approach to extract the initial tsunami profile and, hence, the maximum runup for a simplified beach geometry in terms of earthquake source parameters. In this paper, using regression analysis, we relate the generalized *N*-wave profile as defined by Tadepalli & Synolakis (1996) to the tsunami initial surface profile calculated through Okada's linear elastic dislocation model (Okada 1985) and identify *N*-wave parameters with respect to the earthquake source parameters. Then, we relate tsunami maximum runup to the earthquake source parameters directly through the maximum runup formulation of Tadepalli & Synolakis (1996).

2 *N*-WAVE DEFINED WITH EARTHQUAKE SOURCE PARAMETERS

Tsunamis generated by submarine earthquakes have a finite crest length, and their initial waveform is calculable from estimates of the seismic parameters through Okada's (1985) seafloor deformation. In practice, seafloor deformation is transferred to the sea surface, assuming that the deformation takes place instantaneously. Okada's (1985) linear dislocation model gives sea bottom deformation using a set of seismic parameters, i.e. seismic moment (M_0), fault length (L), fault width (W), fault depth (d), fault slip amount (u), dip angle (δ), rake angle (λ) and strike angle (ϕ) (Fig. 1).

We consider generalized *N*-wave profile

$$\eta(x) = \varepsilon_{1D}\, H\,(x - X_2)\,\mathrm{sech}^2\gamma\,(x - X_1), \tag{1}$$

as in Tadepalli & Synolakis (1996), but in dimensional form. Here, $\varepsilon_{1D} < 1\,(\mathrm{km}^{-1})$ is a scaling parameter to define the initial off-shore wave amplitude of H(m), X_1 (km) and X_2 (km) represent the distance from the origin of the coordinate system, and $\gamma = \sqrt{3\,p_0\,H/4}$ (km^{-1}) with a steepness parameter p_0 ($\mathrm{km}^{-2}\,\mathrm{m}^{-1}$). $X_2 - X_1$ adjusts the initial profile's depression and elevation sides. For small and negative distances $X_2 - X_1$, the generalized *N*-wave profile is an LDN, with a smaller amplitude leading depression wave than the elevation wave following it (see Fig. 2).

Now, we aim to identify relationships between *N*-wave parameters given in eq. (1) and the earthquake source parameters, i.e. $\eta = \eta(x, d, W, \delta, u)$. We consider a large set of submarine earthquake source scenarios and estimate the initial ocean surface profile through Okada's (1985) linear elastic dislocation model (François 2010). The maximum vertical displacement of the sea surface and, consequently, the maximum initial wave height is generated when the rake angle $\lambda = 90^\circ$ (a reverse fault) or $\lambda = -90^\circ$ (a normal fault). We retain the rake angle constant as $\lambda = 90^\circ$ and the strike angle as $\phi = 270^\circ$ to ensure that the tsunami source, the fault's orientation, is parallel to the shoreline and its bisector is 1-D LDN (Fig. 2). Then, we vary the fault slip amount, u, as 1, 5, 10, 15 and 20 m; the fault width, W, from 20 to 150 km by 10 km increments; the fault depth, d, from 5 to 70 km by the interval of 5 km; and the dip angle δ, from 5 to 40° by 5° increments one by one to define a set of earthquake source scenarios (Table 1).

Using 7840 earthquake scenarios, first, we use nonlinear least-squares regression and execute curve fittings to fit the generalized *N*-wave profiles (eq. 1) to the initial surface profiles obtained through Okada (1985) along the bisector, i.e. 1-D fitting. To overlap the *N*-wave profile with Okada's (1985) coordinate system, we set $X_1 = 0$ in eq. (1) in fitting. The depression wave amplitude (trough) decreases with increasing dip angle in the initial profile, almost disappearing at the dip angle of 40°. Jarrard (1986) have pointed out that most megathrust earthquakes have a dip angle of $\delta \leq 40^\circ$. Thus, we exclude such tsunami initial profiles from our database.

We use the fitting results and perform regressions, for example, linear, exponential, logarithmic and power models, to determine the correlation between *N*-wave parameters ε_{1D}, H, X_2 and p_0 and the earthquake source parameters d, W, δ and u. Here, we will only present the final form of our regression results based on the best R^2 values among different regression models. Next, we will explain our methodology in detail and present the summarized results, while Sharghivand (2022) provides details.

2.1 The scaling parameter ε_{1D}

The curve fitting results imply that the scaling parameter ε_{1D} is independent of the slip amount and depends on the fault depth, the fault width and the dip angle, i.e. $\varepsilon_{1D} = \varepsilon_{1D}(d, W, \delta)$. We observe that ε_{1D} decreases logarithmically with the fault depth. Defining the relationship between ε_{1D} and the fault depth as

$$\varepsilon_{1D}(d, W, \delta) = -a_1 \ln d + a_2, \tag{2}$$

we determine a set of $a_1(W, \delta)$ and $a_2(W, \delta)$, using the ε_{1D} and d couplings from the database. Examples of these couplings are given in Fig. 3. We then conduct regression analyses to determine the relationships of $a_1(W, \delta)$ and $a_2(W, \delta)$ with W (Fig. 4), which leads to the following power relations:

$$a_1(W, \delta) = a_3 W^{-a_4} \quad \text{and} \quad a_2(W, \delta) = a_5 W^{-a_6}. \tag{3}$$

Using the coefficients set of $a_3(\delta)$ to $a_6(\delta)$, we further extend the regression analyses and identify their relationships with the dip angle, $a_3(\delta)$ to $a_6(\delta)$ (Fig. 5) as

$$a_3(\delta) = a_7 e^{a_8\delta}, \quad a_4(\delta) = a_9\delta^{a_{10}}, \quad a_5(\delta) = a_{11}e^{a_{12}\delta} \quad \text{and}$$
$$a_6(\delta) = a_{13}\delta^{a_{14}}. \tag{4}$$

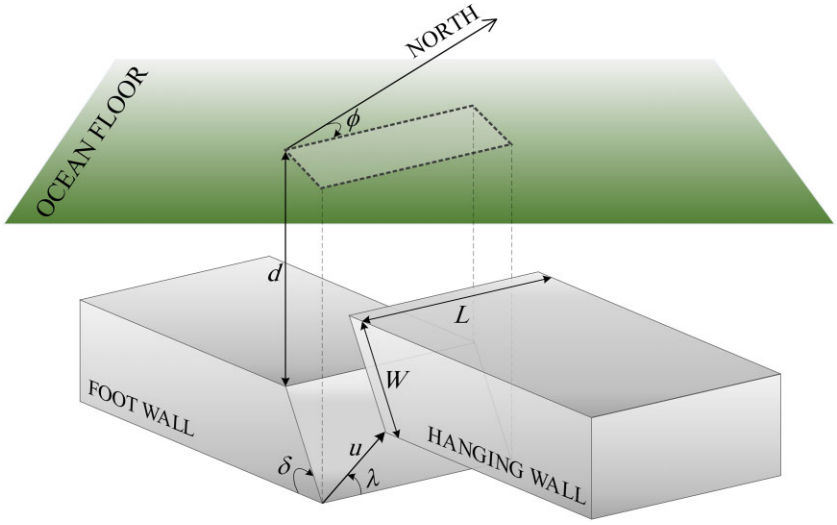

Figure 1. Definition sketch for the fault plane parameters: ϕ, λ and δ are the strike, the rake and the dip angles, respectively; L, W, d and u are the fault length, the fault width, the fault depth and the fault slip amount, respectively.

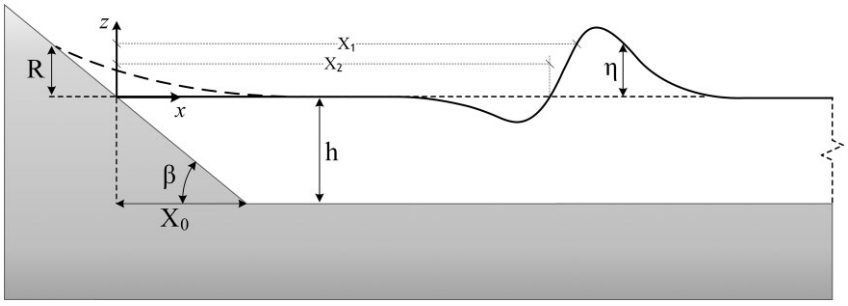

Figure 2. Definition sketch for the canonical problem and N-wave parameters: R is tsunami maximum runup, X_0 is the distance from the coastline to the toe of the sloping beach, $\tan\beta$ is the beach slope, X_1 and X_2 show the distances from the origin of the coordinate system, h is the ocean depth and η is the wave amplitude.

Table 1. The parameter ranges of earthquake source scenarios used in the fitting database.

Fault Plane Parameter	Value
Strike angle (ϕ)	270°
Rake angle (λ)	90°
Dip angle (δ)	5°–40°, 5° increments
Slip amount (u)	1, 5, 10, 15 and 20 m
Fault width (W)	20–150 km, 10 km increments
Fault depth (d)	5–70 km, 5 km increments

This leads to the following estimate for ε_{1D} in terms of the earthquake source parameters:

$$\varepsilon_{1D}(d, W, \delta) = -a_7 e^{a_8\delta}\, W^{-a_9\delta^{a_{10}}}\, \ln d + a_{11} e^{a_{12}\delta}\, W^{-a_{13}\delta^{a_{14}}}. \quad (5)$$

Calculations of a_7 to a_{14} involve error accumulation during the three steps of regression analyses. Hence, we carry out one final nonlinear regression to identify a_7–a_{14} for which eq. (5) best fits to ε_{1D} in the database, resulting as

$$\varepsilon_{1D}(d, W, \delta) = -0.887\, e^{0.005\delta}\, W^{-0.867\delta^{0.089}}\, \ln d + 2.358\, e^{0.0015\delta}\, W^{-0.701\delta^{0.09}}. \quad (6)$$

The goodness-of-fit, R^2, is 0.9929 and the standard deviation of residuals, i.e. the root mean square error (RMSE) is 0.0012 km^{-1} for the final fitting (eq. 6).

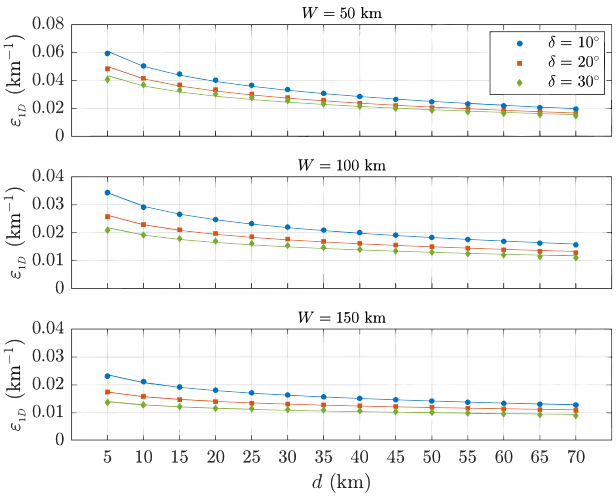

Figure 3. Examples of scaling parameter (ε_{1D}) and fault depth (d) relationships for different fault widths (W) and dip angles (δ), and fitted curves.

2.2 The off-shore wave amplitude H

The relationship between the off-shore wave amplitude H and the fault plane parameters can be described as $H = H(d, W, \delta, u)$. Following the same methodology as described for ε_{1D}, first, we note

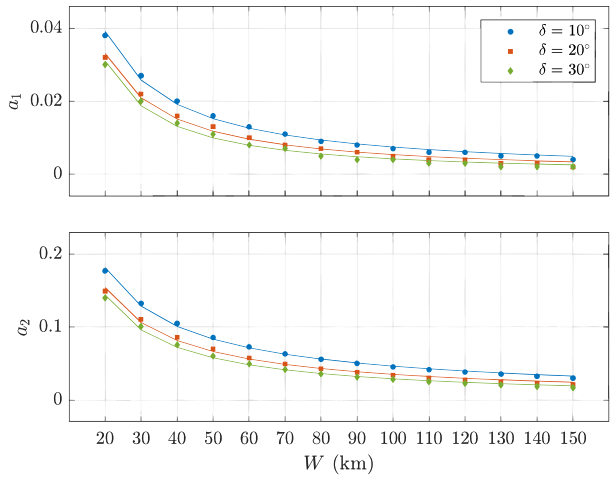

Figure 4. Examples of $a_1(W, \delta)$ and $a_2(W, \delta)$ relationships with fault width (W) for different dip angles (δ), and fitted curves.

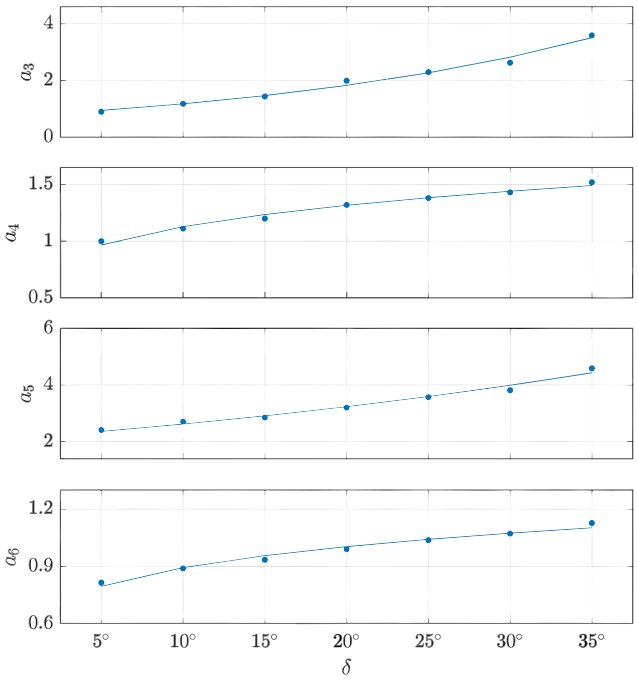

Figure 5. Relationships of $a_3(\delta)$ to $a_6(\delta)$ with dip angle (δ), and fitted curves.

that H exponentially decreases with the fault depth as

$$H(d, W, \delta) = b_1 e^{-b_2 d}. \tag{7}$$

We again perform regression analyses to determine $b_1(W, \delta)$ and $b_2(W, \delta)$ relationships with the fault width, observing that both $b_1(W, \delta)$ and $b_2(W, \delta)$ have power relations with W:

$$b_1(W, \delta) = b_3 W^{b_4} \quad \text{and} \quad b_2(W, \delta) = b_5 W^{-b_6}. \tag{8}$$

Next, we identify the coefficients in eq. (8) in terms of the dip angle as

$$b_3(\delta) = b_7 e^{b_8 \delta}, \quad b_4(\delta) = b_9 \delta^{b_{10}}, \quad b_5(\delta) = b_{11}\delta + b_{12} \quad \text{and} \quad b_6(\delta) = b_{13}\delta + b_{14}. \tag{9}$$

Hence, the regression analyses result defines H as:

$$H(d, W, \delta) = b_7 e^{b_8 \delta}\, W^{b_9 \delta^{b_{10}}}\, e^{-d(b_{11}\delta + b_{12})\, W^{-(b_{13}\delta + b_{14})}}. \tag{10}$$

Performing nonlinear regression once more, we obtain the coefficients b_7–b_{14}. In addition, we observe that H is linearly proportional to the slip amount u. Then, the final representation for H in terms of the earthquake source parameters is:

$$H(d, W, \delta, u) = 0.328\, u\, e^{0.005\delta}\, W^{0.02\delta^{0.44}}\, e^{d\,(0.002\delta - 0.302)\, W^{0.004\delta - 0.794}}, \tag{11}$$

with the R^2 value of 0.9923 and the RMSE of 0.0097 m.

2.3 The distance $X_2 - X_1$

As mentioned earlier, we set $X_1 = 0$ to be consistent with Okada's (1985) coordinate system. Analysing the curve fitting results, we note that X_2 can be explained in terms of the fault depth, the fault width and the dip angle and is not affected by the slip amount, i.e. $X_2 = X_2(d, W, \delta)$. X_2 linearly decreases with increasing fault depth as

$$X_2(d, W, \delta) = c_1 d + c_2. \tag{12}$$

We obtain a set of $c_1(W, \delta)$ and $c_2(W, \delta)$. Then, implementing regression analysis, we define the coefficients against the fault width as

$$c_1(W, \delta) = c_3 W + c_4 \quad \text{and} \quad c_2(W, \delta) = c_5 W + c_6, \tag{13}$$

where the relationships of the coefficients $c_3(\delta)$–$c_6(\delta)$ to the dip angle are:

$$c_3(\delta) \simeq 0, \quad c_4(\delta) = c_7\delta, \quad c_5(\delta) = c_8\delta \quad \text{and} \quad c_6(\delta) = c_9\delta + c_{10}. \tag{14}$$

The outcome defines X_2 in terms of the fault depth, the fault width and the dip angle as

$$X_2(d, W, \delta) = (c_7 d + c_8 W + c_9)\,\delta + c_{10}. \tag{15}$$

Finally, as conducted previously, we determine the value of coefficients from c_7 to c_{10} using nonlinear regression with the R^2 value of 0.9952 and the RMSE of 1.2 km. To align with the generalized N-wave definition (eq. 1), we also include X_1 in the final equation as

$$X_2(d, W, \delta) = (0.1171 - 0.0158\, d - 0.0127\, W)\,\delta - 1.0945 + X_1. \tag{16}$$

X_1 can be used to locate the initial wave at a certain distance from the shoreline, i.e. the initial N-wave profile can be shifted ocean-wise at the distance of X_1.

2.4 The steepness parameter p_0

Analyses results reveal that p_0 is affected by the fault depth, the fault width, the dip angle and the slip amount, i.e. $p_0 = p_0(d, W, \delta, u)$. We identify that the power fit best describes p_0 in terms of the fault depth as

$$p_0(d, W, \delta) = k_1 d^{-k_2}. \tag{17}$$

Again, conducting regression analyses, we first obtain $k_1(W, \delta)$ and $k_2(W, \delta)$ in terms of the fault width:

$$k_1(W, \delta) = k_3 W^{-k_4} \quad \text{and} \quad k_2(W, \delta) = -k_5 \ln W + k_6, \tag{18}$$

where, the relationships of $k_3(\delta)$ to $k_6(\delta)$ with the dip angle are as follows:

$$k_3(\delta) = k_7 e^{k_8\delta}, \quad k_4(\delta) = k_9\delta + k_{10}, \quad k_5(\delta) = k_{11}e^{k_{12}\delta} \quad \text{and}$$
$$k_6(\delta) = k_{13}\delta + k_{14}. \tag{19}$$

Hence, the following equation describes p_0 in terms of the fault depth, the fault width and the dip angle:

$$p_0(d, W, \delta, u) = k_7\, e^{k_8\delta}\, W^{-(k_9\delta+k_{10})}\, d^{k_{11}e^{k_{12}\delta}\ln W - k_{13}\delta - k_{14}}. \tag{20}$$

Further, we note that p_0 is inversely proportional to the slip amount u. Performing nonlinear regression once more, the final form of p_0 becomes:

$$p_0(d, W, \delta, u) = 3.92\, u^{-1}\, e^{0.074\delta}\, W^{-0.022\delta - 1.495} \times d^{0.075\, e^{0.034\delta}\ln W - 0.014\,\delta - 0.776}, \tag{21}$$

with the R^2 of 0.9903 and the RMSE of 0.000237 $\mathrm{km}^{-2}\mathrm{m}^{-1}$.

Substituting eqs (6), (11), (16) and (21) in eq. (1), finally, we define the 1-D form of *N*-wave profile in terms of the earthquake source parameters referring to as the 1-D *N*-wave through earthquake source parameters (NEP):

$$\eta_{\mathrm{NEP}}(x, d, W, \delta, u) = \varepsilon_{1\mathrm{D}}\, H\,(x - X_2)\, \mathrm{sech}^2\gamma\,(x - X_1), \tag{22}$$

where $\varepsilon_{1\mathrm{D}}(d, W, \delta)$, $H(d, W, \delta, u)$, $X_2(d, W, \delta, X_1)$, $p_0(d, W, \delta, u)$, and, hence, $\gamma = \sqrt{3\, p_0\, H/4} = \gamma(d, W, \delta, u)$. Eq. (22) can be used to estimate the initial profile of tsunamis using the earthquake source parameters.

Considering the extension of the generalized *N*-wave profile into two dimensions as in Kânoğlu *et al.* (2013), we extend the 1-D NEP profile eq. (22) into the 2-D profile as

$$\eta_{\mathrm{NEP}}(x, y, d, W, L, \delta, u) = \frac{1}{2}\,\varepsilon_{2\mathrm{D}}\, H\,(x - X_2)\, \mathrm{sech}^2\gamma\,(x - X_1) \times[\tanh\gamma\,(y + L/2) - \tanh\gamma\,(y - L/2)], \tag{23}$$

where L refers to the initial wave crest length, which is equal to the earthquake fault length. We determine that varying the fault length directly affects the initial tsunami wave's crest length, and its effect on the initial wave height is negligible. $\varepsilon_{2\mathrm{D}}$ can be defined as

$$\varepsilon_{2\mathrm{D}} = 2\,\varepsilon_{1\mathrm{D}}/[\tanh(\gamma L/2) - \tanh(-\gamma L/2)], \tag{24}$$

where $\varepsilon_{1\mathrm{D}}$ is given with eq. (6). Substitution of eqs (24), (11), (16) and (21) into eq. (23) will provide the 2-D *N*-wave profile in terms of the earthquake source parameters. We provide an example for the comparison of a 2-D NEP profile with the individually fitted *N*-wave profile and their corresponding Okada's (1985) displacement model in Fig. 6.

3 MAXIMUM RUNUP THROUGH EARTHQUAKE SOURCE PARAMETERS

This far, we have defined the tsunami initial profile with respect to the fault plane parameters. Next, we aim to determine the tsunami maximum runup in terms of the earthquake source parameters. Here, we use the undisturbed ocean depth h as the reference depth, either in m (h_m) or in km (h_{km}) dimensions, to introduce the non-dimensional variables as

$$\tilde{\eta}, \tilde{H}, \tilde{R} = (\eta, H, R)/h_m, \quad \tilde{X}_0, \tilde{X}_1, \tilde{X}_2, \tilde{L} = (X_0, X_1, X_2, L)/h_{km}, \quad \tilde{p}_0 = p_0 \times (h_{km})^2 \times h_m \quad \text{and} \quad \tilde{\varepsilon}_{1\mathrm{D}} = \varepsilon_{1\mathrm{D}} \times h_{km}. \tag{25}$$

Tadepalli & Synolakis (1994) used the solution methodology of Synolakis (1986) and solved the linear shallow-water wave equations to obtain the evolution of several types of *N*-waves over a canonical bathymetry. They performed asymptotic analysis and expressed tsunami runup laws for different initial *N*-wave forms. Tadepalli & Synolakis (1994) computed an approximate upper bound for runup of the non-breaking LDNs.

Further, Tadepalli & Synolakis (1994) introduced the steepness parameter in the definition of *N*-wave to represent initial tsunami profile more realistically, however, they did not provide the approximate upper bound of the runup explicitly as in Tadepalli & Synolakis (1994). They calculated the runup of *N*-wave profile (1) as

$$\tilde{R}(\tilde{t}) = \frac{16}{3}\tilde{\varepsilon}_{1\mathrm{D}}\tilde{\gamma}_s^{3/2}(2\pi\tilde{X}_0)^{1/2}\left(\frac{1}{\tilde{p}_0^{1/4}}\right)\sum_{n=1}^{\infty}(-1)^{n+1}n^{1/2} \times\left\{2n\tilde{\gamma}\,(\tilde{X}_1 - \tilde{X}_2 - \tilde{\phi}) + \frac{1}{2}\right\}e^{-2n\tilde{\gamma}\tilde{\phi}}, \tag{26}$$

where $\tilde{\gamma}_s = \sqrt{3\tilde{H}/4}$, $\tilde{X}_0 = \cot\beta$ (distance from the shoreline to toe of the sloping beach in canonical topography and β is the beach slope), $\tilde{\phi} = \tilde{X}_1 + \tilde{X}_0 - \tilde{c}\tilde{t}$, and with normalization $\tilde{c} = 1$. We use the same approach as Synolakis (1987) and Tadepalli & Synolakis (1994) and calculate an approximate upper bound as

$$\tilde{R}_{REP}(d, W, \delta, u) = 2.831\tilde{\varepsilon}_{1\mathrm{D}}\sqrt{\tilde{X}_0}\tilde{H}^{5/4}\tilde{p}_0^{1/4} \times\left[\left|\tilde{X}_1 - \tilde{X}_2 - \frac{0.366}{\tilde{\gamma}}\right| + \frac{0.618}{\tilde{\gamma}}\right]. \tag{27}$$

Eq. (27) is valid when $4\tilde{\gamma}\tilde{X}_0 \gg 1$ and $\tilde{H} < \tilde{H}_{\mathrm{breaking}}$, i.e. non-breaking waves.

We substitute the non-dimensional form of eqs (6), (11), (16) and (21) into eq. (27) to provide the approximate maximum runup for a 1-D NEP profile (eq. 22). The resulting equation eq. (27) is referred to hereafter as runup through earthquake parameters (REP). We compare maximum runup values calculated through REP with those computed using the $\varepsilon_{1\mathrm{D}}$, H, X_2 and p_0 parameters obtained through the fitting database for 240 different earthquake source scenarios and observe good agreement (Fig. 7).

4 FIELD VALIDATION

Now, we will test REP (eq. 27) comparing with the field runup measurements for several events. We use 1-D NEP to obtain the initial waveforms of the Nicaragua 1992; the Indonesia, Java 1994; the Mexico, Colima 1995; the Sumatra 2004; the Chile, Maule 2010; the Japan, Tohoku 2011; and the Aegean Sea, Turkey 2020 tsunamis (Table 2, including corresponding references). We then calculate tsunami runup values for these events using REP, and compare them with the mean and extreme field runup measurements, which were acquired through the National Geophysical Data Center/World Data Service: NGDC/WDS (2022). Further, we have obtained the field runup measurements for the 2020 Aegean Sea event from Doğan *et al.* (2021). The beach slope ($\tan\beta$) and the ocean depth (h) for Sumatra 2004 and Chile 2010 events have been considered as in Sepúlveda & Liu (2016). The ocean depth and the beach slope are approximated using the General Bathymetric Chart of the Oceans (GEBCO 2020) bathymetry for the 2011 Tohoku and the 2020 Turkey tsunamis. For other events, the referred parameters are the same as Wronna *et al.* (2021).

We compute initial wave profiles using 1-D NEP and compare them with Okada's (1985) dislocation model results using the earthquake source parameters, given in Table 2. All initial wave profiles estimated from NEP fit well with Okada's (1985) model (Fig. 8). Further, runup estimations based on REP are compatible with post-events field runup measurements (Fig. 9 and Table 2). Although

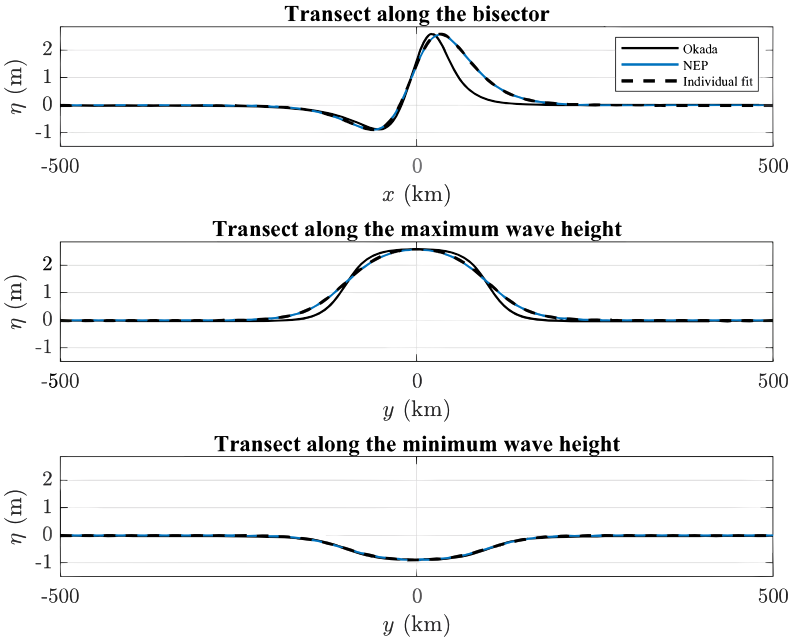

Figure 6. Two-dimensional NEP profile (blue solid line; grey in black/white version) compared with the individually fitted *N*-wave profile (black dashed line) and Okada's (1985) displacement model (black solid line) using the submarine earthquake source with $L = 200$ km, $W = 50$ km, $d = 40$ km, $u = 10$ m, $\delta = 20^\circ$, $\lambda = 90^\circ$ and $\phi = 270^\circ$. RMSEs between NEP and Okada profiles from top to bottom are calculated as 0.26, 0.13 and 0.02 m, respectively.

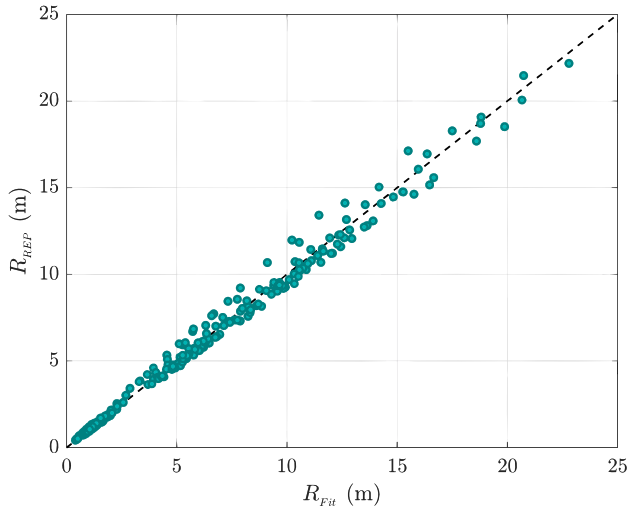

Figure 7. Comparison of runup estimates calculated using REP (eq. 27) with those calculated using the parameters in fitting database. The earthquake source scenarios are defined by varying parameters as $W = 20,\ 50,\ 100$ and 150 km, $d = 10,\ 20,\ 30$ and 40 km, $u = 1,\ 5$ and 10 m, $\delta = 10^\circ$–30° with 5° increments, and the beach slope of 1/20.

there are a limited number of events, we perform statistical analysis using a two-tailed Student's *t*-test at a significance level of $\alpha = 0.05$ to compare the mean field runup measurements and the REP results for different events. The null hypothesis states that there is no statistically significant difference between the mean field runup measurements and the corresponding REP values. We calculate a *P*-value of 0.36 greater than α of 0.05, implying that the null hypothesis is accepted. Following, we summarize our observations.

We calculate a runup height of 9.5 m for the 1992 Nicaraguan tsunami, which is within the mean and extreme field runup measurements (6.8–9.9 m). For the Java 1994 tsunami, the runup calculated by REP is about 8 m (1.5 m less than the mean runup value), yet between the minimum 5.4 m and maximum 13.9 m runup values of field observations, which have been reported only at four locations (Synolakis *et al.* 1995; Maramai & Tinti 1997; NGDC/WDS 2022).

For the Mexico, Colima 1995 event, the REP is in line with the post-event field surveys measurements with a runup height of 6.6 m. While Borrero *et al.*'s (2006) post-tsunami field survey measurements in northern Sumatra in the region around Banda Aceh identified the runup variation between 2.5 and 31 m for the 2004 Sumatra tsunami, NGDC/WDS (2022) reports 13.1 m and 40.2 m mean and extreme runup field measurements, respectively. We use the same rupture parameters as Sepúlveda & Liu (2016) for the event, who calculated a runup height of 7.8 m using the moment-based rupture parameters. The REP estimates a runup height of 9.7 m, in between the minimum and maximum field runup measurements, underestimating the mean field runup value. In the 2010 Chile Maule field survey, maximum runup heights of 29 m along a steep coastal bluff at Constitución and 20 m in a coastal bluff within 70 m of the shoreline to the south of the Tirúa river have been reported (Fritz *et al.* 2011). The measurements indicate that, except in bluff landforms, the tsunami maximum runup values were 5–15 m, while between Constitución and Punta Morguilla 5–15 m, in the regions between Punta Morguilla and Mehuín mostly under 5 m, and in the Greater Valparaíso area below 5 m. The REP runup height of 12.2 m is in accordance with the post-event field observations, while Sepúlveda & Liu's (2016) runup result is 11.7 m for the event. The magnitude M_w 9.1, 2011 March 11 East Japan earthquake generated one of the most destructive tsunamis in recorded history. A massive tsunami penetrated the Pacific coast of Japan. The runup height reached 16.4 and 20.8 m at the distance of 30 and 40 km from the nuclear power plant, respectively and the extreme runup height of 39.7 m was

Table 2. The source parameters and beach slopes used for the events. Here, M_w, u, W, d and δ indicate the moment magnitude, the slip amount, the fault width, the fault depth and the dip angle, respectively; tan β represents the nearshore beach slope and h is the ocean depth. R_{REP} is calculated using eq. (27), and R_{Mean} and R_{Ext} show the mean and extreme filed runup measurements for the events, respectively. The mean and extreme field runup measurements are obtained through NGDC/WDS (2022).

Event	References	M_w	u (m)	W (km)	d (km)	δ (°)	tan β	h (m)	R_{REP} (m)	Field measurements	
										R_{Mean} (m)	R_{Ext} (m)
Nicaragua 1992	Wronna *et al.* (2021)										
	Okal & Synolakis (2004)										
	Piatanesi *et al.* (1996)										
	Dziewonski *et al.* (1995)	7.7	5.00	100	16	12	1/29	4814	9.5	6.8	9.9
Indonesia, Java 1994	Wronna *et al.* (2021)										
	Okal & Synolakis (2004)										
	Abercrombie *et al.* (2001)										
	Dziewonski *et al.* (1995)	7.8	3.40	80	16	12	1/57	3294	8.0	9.5	13.9
Mexico, Colima 1995	Wronna *et al.* (2021)										
	Okal & Synolakis (2004)										
	Mendoza & Hartzell (1999)										
	Dziewonski *et al.* (1997)	8.0	4.30	100	15	9	1/18	3844	6.6	4.3	10.9
Sumatra, Aceh 2004	Sepúlveda & Liu (2016)										
	NEIC	9.3	10.22	150	30	10	1/34	1500	9.7	13.1	40.2
Chile, Maule 2010	Sepúlveda & Liu (2016)										
	NEIC	8.8	10.05	100	30	20	1/32	3100	12.2	8.4	29.0
Japan, Tohoku 2011	NEIC										
	Duputel *et al.* (2012)	9.1	19.00	100	11.5	9	1/34	1500	26.5	11.3	39.7
Aegean Sea, Turkey 2020	NEIC	7.0	1.50	15	11.5	29	1/50	480	1.8	1.5	3.8

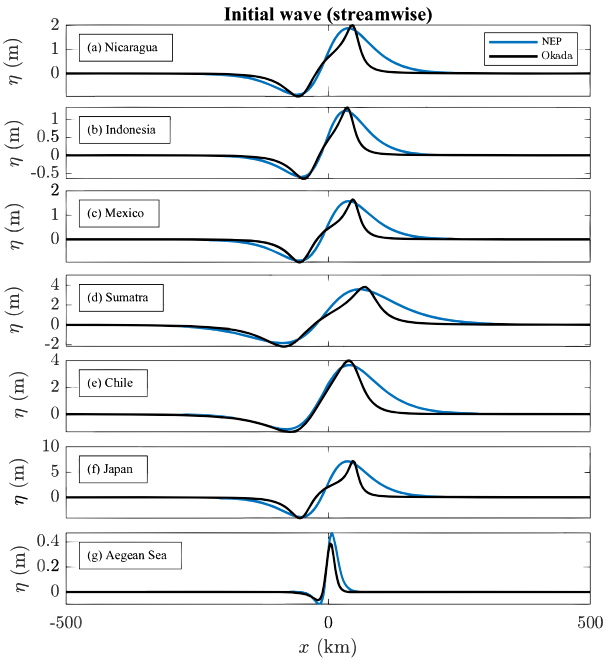

Figure 8. Leading depression initial waveform through NEP (grey in black/white version) and Okada (1985) for (a) the Nicaragua 1992; (b) the Indonesia, Java 1994; (c) the Mexico, Colima 1995; (d) the Sumatra 2004; (e) the Chile, Maule 2010; (f) the Japan, Tohoku 2011 and (g) the Aegean Sea, Turkey 2020 tsunamis. The fault plane parameters for the events and references are provided in Table 2.

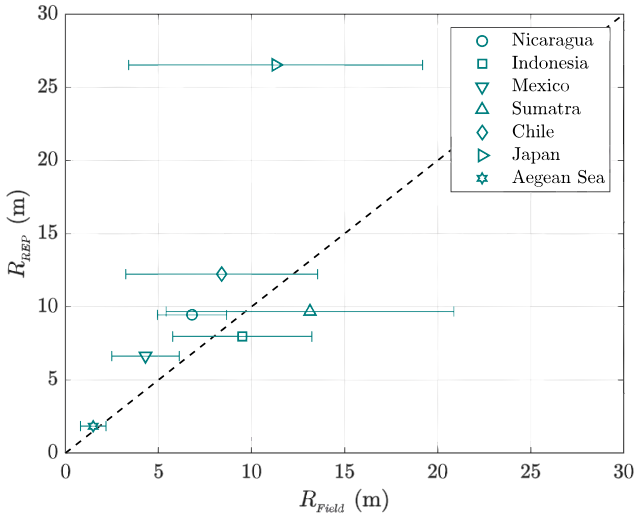

Figure 9. Comparison of runup values calculated using REP (eq. 27) with the mean field runup measurements. The error bars indicate standard deviations from the mean field runup values. The fault plane parameters for the events and references are provided in Table 2. The mean field runup measurements are acquired through NGDC/WDS (2022).

measured at Aneyoshi, Miyako (Mori *et al.* 2011). We computed a runup height of 26.5 m using the REP, which is in the range of mean and extreme field runup measurements (11.3–39.7 m). We utilize the earthquake source model provided by National Earthquake Information Center (NEIC) (Sipkin *et al.* 2000) for the Aegean Sea, Turkey 2020 event. The REP estimates a runup height of 1.8 m, which is in agreement with the mean and extreme field runup observations (1.5–3.8 m) along the Turkish coast reported by Doğan *et al.* (2021). This runup value is also very close to the runup values, 1.2–3 m reported on five Greek islands (Kalligeris *et al.* 2022).

5 CONCLUSIONS

We related the earthquake source parameters to the initial tsunami wave and the maximum runup presenting generalized *N*-wave profile in terms of earthquake source parameters. We justified our results by comparing them with field runup measurements of the the 1992 Nicaragua, the 1994 Indonesia, the 1995 Mexico, the 2004

Sumatra, the 2010 Chile, the 2011 Japan and the 2020 Aegean Sea tsunamis. Our approach can provide a quick estimate of the tsunami maximum runup height whenever the fault plane parameters of the tsunami source are available or estimated.

Even though we reasonably varied the earthquake fault plane parameters for the fitting processes to cover the most probable earthquake scenarios, results should not be used whenever the earthquake fault plane parameters are outside the range of the fitting database. Also, REP provides a runup estimate for canonical bathymetry; complexities in the maximum runup, e.g. bottom friction, complex beach slope and 3-D coastal morphology are not considered here. Nonetheless, our approach can provide a reasonable tsunami runup estimate, especially where the high-resolution geospatial data are unavailable, and whenever a quick early warning is needed.

ACKNOWLEDGMENTS

NS would like to thank Associate Prof Dr Baran Aydın for his valuable support during this study. This research is partially funded by project ASTARTE—Assessment, STrategy And Risk Reduction for Tsunamis in Europe-7th FP ENV.2013.6.4-3, grant 603839.

DATA AVAILABILITY

The fitting database is available in the Zenodo repository at https://doi.org/10.5281/zenodo.7826204

REFERENCES

Abercrombie, R.E., Antolik, M., Felzer, K. & Ekström, G., 2001. The 1994 Java tsunami earthquake: slip over a subducting seamount, *J. Geophys. Res. Solid Earth,* **106**(B4), 6595–6607.

Aydın, B. & Kânoğlu, U., 2017. New analytical solution for nonlinear shallow water-wave equations, *Pure Appl. Geophys.,* **174**(8), 3209–3218.

Aydın, B., Sharghivand, N. & Özgen, B., 2020. Potential tsunami hazard along the southern Turkish coast, *Coast. Eng.,* **158,** 103696.

Baba, T., Takahashi, N. & Kaneda, Y., 2014. Near-field tsunami amplification factors in the Kii Peninsula, Japan for Dense Oceanfloor Network for Earthquakes and Tsunamis (DONET), *Mar. Geophys. Res.,* **35**(3), 319–325.

Behrens, J., Løvholt, F., Jalayer, F., Lorito, S., Salgado-Gálvez, M.A. & Sørensen, M., 2022. *Assessing research gaps in probabilistic tsunami hazard and risk analysis,* Tech. Rep., Copernicus Meetings.

Borrero, J., Yalçiner, A.C., Kanoglu, U., Titov, V., McCarthy, D. & Synolakis, C., 2003. *Producing Tsunami Inundation Maps: the California Experience,* pp. 315–326, Springer Netherlands, Dordrecht.

Borrero, J.C., Synolakis, C.E. & Fritz, H., 2006. Northern Sumatra field survey after the December 2004 great Sumatra earthquake and Indian Ocean tsunami, *Earthq. Spectra,* **22**(S3), 93–104.

Davies, G. & Griffin, J., 2019. Sensitivity of probabilistic tsunami hazard assessment to far-field earthquake slip complexity and rigidity depth-dependence: case study of Australia, *Pure Appl. Geophys.,* **177**(3), 1521–1548.

Doğan, G.G., *et al.* 2021. The 30 October 2020 Aegean Sea tsunami: post-event field survey along Turkish coast, *Pure Appl. Geophys.,* **178,** 785–812.

Duputel, Z., Rivera, L., Kanamori, H. & Hayes, G., 2012. W phase source inversion for moderate to large earthquakes (1990–2010), *Geophys. J. Int.,* **189**(2), 1125–1147.

Dziewonski, A., Ekström, G. & Salganik, M., 1995. Centroid-moment tensor solutions for April–June 1994, *Phys. Earth Planet. Inter.,* **88**(2), 69–78.

Dziewonski, A., Ekström, G. & Salganik, M., 1997. Centroid-moment tensor solutions for October–December 1995, *Phys. Earth Planet. Inter.,* **101**(1), 1–12.

François, B., 2010. *Okada: Surface deformation due to a finite rectangular source, Matlab code, MATLAB Central File Exchange*.

Fritz, H.M. *et al.*, 2011. Field survey of the 27 February 2010 Chile tsunami, *Pure Appl. Geophys.,* **168**(11), 1989–2010.

GEBCO, 2020. *GEBCO bathymetric compilation group 2020, the GEBCO 2020 grid—a continuous terrain model of the global oceans and land,* https://download.gebco.net/, Accessed 2022 April.

Geist, E.L., 1998. Local tsunamis and earthquake source parameters, in *Adv. Geophys.,* Vol. **39,** pp. 117–209, Elsevier.

Glimsdal, S. *et al.*, 2019. A new approximate method for quantifying tsunami maximum inundation height probability, *Pure Appl. Geophys.,* **176**(7), 3227–3246.

González, F. *et al.*, 2009. Probabilistic tsunami hazard assessment at Seaside, Oregon, for near-and far-field seismic sources, *J. Geophys. Res. Oceans,* **114**(C11).

Grezio, A. *et al.*, 2017. Probabilistic tsunami hazard analysis: multiple sources and global applications, *Rev. Geophys,* **55**(4), 1158–1198.

Harbitz, C.B. *et al.*, 2016. Risk assessment and design of prevention structures for enhanced tsunami disaster resilience (RAPSODI)/Euro-Japan collaboration, *Coast. Eng.,* **58**(4), 1640012–1-1640012-37.

Imamura, F. & Imteaz, M.A., 1995. *Long waves in two layers: governing equations and numerical model*. http://hdl.handle.net/1959.3/54053, Accessed 2023 May

Jarrard, R.D., 1986. Relations among subduction parameters, *Rev. Geophys.,* **24**(2), 217–284.

Kalligeris, N., Skanavis, V., Charalampakis, M., Melis, N., Voukouvalas, E., Annunziato, A. & Synolakis, C., 2022. Field survey of the 30 October 2020 Samos (Aegean Sea) tsunami in the Greek islands, *Bull Earthq Eng.,* **20**(14), 7873–7905.

Kânoğlu, U., 2004. Nonlinear evolution and runup-rundown of long waves over a sloping beach, *J. Fluid Mech,* **513,** 363–372.

Kânoğlu, U., Titov, V.V., Aydın, B., Moore, C., Stefanakis, T.S., Zhou, H., Spillane, M. & Synolakis, C.E., 2013. Focusing of long waves with finite crest over constant depth, *Proc. R. Soc. A—Math. Phys. Eng. Sci.s,* **469**(2153).

Kânoğlu, U., Titov, V., Bernard, E. & Synolakis, C., 2015. Tsunamis: bridging science, engineering and society, *Philos. Trans. R. Soc. A,* **373**(2053), 20140369.

Liu, P. L.-F., Woo, S.-B. & Cho, Y.-S., 1998. Computer programs for tsunami propagation and inundation, *Cornell University,* **25**.

Løvholt, F., Griffin, J. & Salgado-Gálvez, M., 2016. *Tsunami Hazard and Risk Assessment on the Global Scale,* pp. 1–34, Springer, Berlin, Heidelberg.

Løvholt, F., Glimsdal, S., Harbitz, C.B., Zamora, N., Nadim, F., Peduzzi, P., Dao, H. & Smebye, H., 2012. Tsunami hazard and exposure on the global scale, *Earth Sci. Rev.,* **110**(1), 58–73.

Lynett, P.J. *et al.*, 2017. Inter-model analysis of tsunami-induced coastal currents, *Ocean Model (Oxf),* **114,** 14–32.

Madsen, P.A. & Schäffer, H.A., 2010. Analytical solutions for tsunami runup on a plane beach: single waves, *N*-waves and transient waves, *J. Fluid Mech,* **645,** 27–57.

Maramai, A. & Tinti, S., 1997. The 3 June 1994 Java tsunami: a post-event survey of the coastal effects, *Nat. Hazards,* 31–49.

Mendoza, C. & Hartzell, S., 1999. Fault-slip distribution of the 1995 Colima-Jalisco, Mexico, earthquake, *Bull. Seismol. Soc. Am.,* **89**(5), 1338–1344.

Miranda, J. & Luis, J., 2019. *NSWING (Non-linear Shallow Water Model with Nested Grids), Instituto Dom Luiz*.

Miranda, J., Luis, J., Reis, C., Omira, R. & Baptista, M.A., 2014. Validation of NSWING, a multi-core finite difference code for tsunami propagation and run-up, in *AGU fall meeting,* San Francisco, Paper, no. S21A-4390.

Mori, N., Takahashi, T., Yasuda, T. & Yanagisawa, H., 2011. Survey of 2011 Tohoku earthquake tsunami inundation and run-up, *Geophys. Res. Lett.,* **38**(7).

NGDC/WDS, 2022. *Global historical tsunami database. National Geophysical Data Center NOAA, Accessed 2022 February*.

Okada, Y., 1985. Surface deformation due to shear and tensile faults in a half-space, *Bull. Seism. Soc. Am.,* **75**(4), 1135–1154.

Okal, E. & Synolakis, C., 2004. Source discriminants for near-field tsunamis, *Geophys. J. Int.,* **158**(3), 899–912.

Piatanesi, A., Tinti, S. & Gavagni, I., 1996. The slip distribution of the 1992 Nicaragua earthquake from tsunami run-up data, *Geophys. Res. Lett.,* **23**(1), 37–40.

Schlurmann, T., Kongko, W., Goseberg, N., Natawidjaja, D. & Sieh, K., 2010. Near-field tsunami hazard map Padang, West Sumatra: utilizing high resolution geospatial data and reseasonable source scenarios, *Coast. Eng.,* **2**.

Sepúlveda, I. & Liu, P. L.-F., 2016. Estimating tsunami runup with fault plane parameters, *Coast. Eng.,* **112,** 57–68.

Sepúlveda, I., Liu, P. L.-F. & Grigoriu, M., 2019. Probabilistic tsunami hazard assessment in South China Sea with consideration of uncertain earthquake characteristics, *J. Geophys. Res.: Solid Earth,* **124**(1), 658–688.

Sharghivand, N., 2022. *Tsunami maximum runup and focusing through earthquake source parameters,* Ph.D. thesis, Middle East Technical University, Ankara, Turkey.

Sipkin, S., Person, W. & Presgrave, B., 2000. Earthquake bulletins and catalogs at the USGS National Earthquake Information Center (NEIC), *IRIS Newsl.,* **2000**(1), 2–4.

Synolakis, C., 1986. *The runup of long waves,* Ph.D. thesis, California Institute of Technology, Engineering and Applied Science, Pasadena, California, USA.

Synolakis, C., 1987. The runup of solitary waves, *J. Fluid Mech,* **185,** 523–545.

Synolakis, C.E. & Bernard, E.N., 2006. Tsunami science before and beyond Boxing Day 2004, *Philos. Trans. Royal Soc. A,* **364**(1845), 2231–2265.

Synolakis, C.E., Imamura, F., Tsuji, Y., Matsutomi, H., Tinti, S., Cook, B., Chandra, Y.P. & Usman, M., 1995. Damage, conditions of East Java tsunami of 1994 analyzed, *EOS, Trans. Am. Geophys. Un.,* **76**(26), 257–257.

Tadepalli, S. & Synolakis, C., 1994. The run-up of *N*-waves on sloping beaches, *Proc. Math. Phys. Eng. Sci.,* **445**(1923), 99–112.

Tadepalli, S. & Synolakis, C., 1996. Model for the leading waves of tsunamis, *Phys. Rev. Lett.,* **77**(10), 2141–2144.

Tang, L. *et al.*, 2012. Direct energy estimation of the 2011 Japan tsunami using deep-ocean pressure measurements, *J. Geophys. Res. Oceans,* **117**(C8).

Tinti, S. & Tonini, R., **13** 2013. 1795–-1816 The UBO-TSUFD tsunami inundation model: validation and application to a tsunami case study focused on the city of Catania, Italy, *Nat. Hazards Earth Syst. Sci*.

Titov, V., Rabinovich, A.B., Mofjeld, H.O., Thomson, R.E. & González, F.I., 2005. The global reach of the 26 December 2004 Sumatra tsunami, *Science,* **309**(5743), 2045–2048.

Titov, V., Kânoğlu, U. & Synolakis, C., 2016. Development of MOST for real-time tsunami forecasting, *J. Waterw. Port Coast. Ocean Eng.,* **142**(6), 03116004.

Walsh, T.J., Titov, V.V., Venturato, A.J., Mofjeld, H.O. & Gonzalez, F.I., 2004. Tsunami hazard map of the Bellingham area, Washington: modeled tsunami inundation from a Cascadia subduction zone earthquake, in *Washington Division of Geology and Earth Resources Open File Report,* Vol. **15**(40), p. 36.

Wronna, M., Baptista, M.A. & Kânoğlu, U., 2021. A new tsunami runup predictor, *Nat. Hazards,* **105**(2), 1571–1585.

Yalçıner, A.C. *et al.*, 2019. Complete tsunami hazard assessment, vulnerability and risk analysis for the Marmara coast of Istanbul metropolitan area, *Geophys. Res. Abstr.,* **21,** 1. *EGU General Assembly Conference Abstracts*